Ferroelectricity in a quasiamorphous ultrathin BaTiO₃ film

J. L. Wang,[1] A. Pancotti,[1,2] P. Jégou,[3] G. Niu,[4] B. Gautier,[5] Y. Y. Mi,[1] L. Tortech,[6,7] S. Yin,[4] B. Vilquin,[4] and N. Barrett[1,*]

[1]*IRAMIS/SPCSI/LENSIS, FR-91191 Gif-sur-Yvette, France*

[2]*Departamento de Física Aplicada, Universidade Estadual de Campinas, Caixa Postal 6165, 13083-970, Campinas, SP, Brazil*

[3]*IRAMIS/SPCSI/LCSI, FR-91191 Gif-sur-Yvette, France*

[4]*Université de Lyon, Ecole Centrale de Lyon, Institut des Nanotechnologies de Lyon, FR-69134 Ecully cedex, France*

[5]*Université de Lyon, INSA Lyon, Institut des Nanotechnologies de Lyon, FR-69621 Villeurbanne cedex, France*

[6]*CEA, IRAMIS, SPCSI, LEPO, FR-91191 Gif sur Yvette cedex, France*

[7]*Institut Parisien de Chimie Moléculaire (UMR CNRS 7201), UPMC Université Paris 06, 4 Place Jussieu, C. 229, FR-75005 Paris, France*

Until now, the quasiamorphous (QA) phase in BaTiO₃ (BTO), SrTiO₃ (STO), and BaZrO₃ was achieved by pulling a thick film through a steep temperature gradient. Here, we show that a room-temperature deposited ultrathin film, subsequently annealed in O₂ can also produce a QA phase. The atomic, electronic, and ferroelectric (FE) structure of a QA, ultrathin BTO grown on STO were studied by x-ray diffraction (XRD), x-ray photoelectron diffraction (XPD), x-ray photoelectron spectroscopy (XPS), and piezoforce microscopy (PFM). The absence of long-range order is confirmed by in- and out-of-plane XRD as well as Ti $2p$ XPD. FE polarized domains with good retention have been successfully written into the QA film and exhibit a clear P-E hysteresis loop. Substrate clamping frustrates volume expansion during annealing leading to a QA film. Photoelectron spectroscopy confirms a similar overall electronic structure as for thicker films but with some significant differences. Simple charge-transfer arguments are not sufficient to explain the high-resolution core-level spectra. Ba, Ti, and O all show components associated with a surface region. We suggest that the observation of such a component in the Ti $2p$ spectrum is linked with the high dynamic charge tensor induced by the large off-center displacement of the Ti ion.

PACS number(s): 68.55.−a, 68.37.−d, 77.80.bn

I. INTRODUCTION

Ferroelectric (FE) materials have attracted much attention, not only because of their fascinating electronic properties, but also because of promising applications in electronic devices such as nonvolatile FE memories. They are therefore of both fundamental scientific interest and great practical importance.[1,2] However, the search for new polar materials is largely empirical. For a long time, it was believed that spontaneous polarization existed only in ionic crystals due to a noncentrosymmetrical spatial distribution of ions in a polar crystalline structure. This commonly accepted idea now needs to be reconsidered following the discovery of noncrystalline pyro- and piezoelectric-phase thin films of BaTiO₃ (BTO), SrTiO₃ (STO), and BaZrO₃ (BZO).[3,4] The subsequent investigation of this new phase, called quasiamorphous (QA), revealed that the amorphous material contains a network of randomly connected, slightly distorted octahedral local bonding units (LBU), such as TiO₆ or ZrO₆, that can be polarized along an axis corresponding to the strain in 50–250 nm films on Si or SiO₂ during annealing.[5–10] The material must contain one cation forming stable LBUs and a second cation capable of stabilizing underbonded oxygen. X-ray absorption near edge spectroscopy (XANES) has been used to determine the Ti off-center displacement of 0.44 Å.[7] Extended x-ray absorption spectroscopy of the QA phase showed that the TiO₆ octahedra are deformed by less than 4%. The TiO₆ octahedra are both apex and edge sharing in the amorphous and QA phases. The polarity is the result of the orientational ordering of the LBUs without any detectable spatial long-range order. Alignment of 5% of the LBUs is sufficient to create a macroscopic polarization. This opens up a new direction for FE material

design no longer limited to crystalline compounds. However, to our knowledge, ferroelectricity in quasiamorphous phases has not yet been reported nor has the QA phase in ultrathin device compatible films been observed.

In this paper, piezoforce microscopy (PFM) has been used to write and read stable ferroelectric domains on such a QA film. The phase signal image shows a clear electrical contrast, corresponding to stable, antiparallel FE domains.[11] P-E hysteresis demonstrates that the ultrathin QA BTO film is ferroelectric. X-ray diffraction (XRD) proves the absence of long-range order. Angle-scanned x-ray photoelectron diffraction (XPD) is a well established tool for surface structure determination[12] combining chemical sensitivity with quantitative information on the local atomic structure around each emitting atom with a precision of approximately ±0.02 Å. It is therefore ideal to probe elemental-specific local distortions at the surface of ferroelectric materials and is used to confirm the amorphous nature of the QA film. X-ray photoelectron spectroscopy (XPS) is sensitive to the first few nm below the surface and is thus an ideal tool for studying the chemical and electronic structure of thin films. Here, it reveals significant differences between the ultrathin QA film and the thicker films already reported.[10] The results establish a method to form ultrathin, quasiamorphous ferroelectric BTO on STO by homogeneous postannealing in O₂ flow.

II. EXPERIMENT

The commercial STO(001) substrate with an optical mirror surface finish was etched with buffered NH₄F-HF solution (BHF) of pH ~5.5 for 10 min, rinsed by deionized water and dried in N₂ stream. Then it was annealed at 950 °C

in O_2 flow for 10 hours to obtain the TiO_2 termination surface composed of one unit-cell steps and atomically flat terraces following the established protocol.[13] After heating the substrate to 650 °C for 1 hour under an oxygen partial pressure of $\sim 10^{-6}$ Torr to remove carbon contamination on the surface, two ultrathin BTO films were grown on these substrates by molecular beam epitaxy (MBE) with a growth rate of $\sim$0.5 monolayers (ML)/min and $\sim$1 ML/min, respectively. The metallic Ba and Ti were put in the Knudsen cells heated by a resistance coil to produce the vapor flux. During growth, the oxygen partial pressure was kept at 2×10^{-6} Torr and the substrates were maintained at room temperature. After deposition, the samples were annealed at 700 °C in O_2 flow for 1 hour. The crystalline or amorphous state of the samples was measured by high-resolution x-ray diffraction (six-circles Rigaku SmartLab diffractometer with rotative anode using Cu KαI line, $\lambda = 1.5406$ Å) in the θ-2θ mode for in-plane and out-of-plane scans. XPD was conducted on ANTARES beam line at SOLEIL synchrotron. To determine the film structure, the Ti $2p$ XPD emission was measured over a wide range of polar and azimuthal angles with an angular resolution of $\pm 1°$. The photon energy was 900 eV giving low photoelectron kinetic energies and enhanced surface sensitivity. XPS was carried out using a Kratos Ultra DLD with monochromatic Al Kα (1486.7 eV). The analyzer pass energy of 20 eV gave an overall energy resolution (photons and spectrometer) of 0.35 eV. The sample is at floating potential and a charge compensation system was used. The binding energy scale was calibrated using the C-1s line at 284.6 eV as a reference. A take-off angle of 90°, i.e., normal emission, was used for all analyses presented. Thus the XPS probes the full BTO film thickness. Grazing angle emission was used to check the surface nature of the core-level peaks. The data were analyzed using the CASAXPS software,[14] which employs a linear least-squares optimization with a peak-fitting algorithm. Shirley backgrounds were used and subtracted from the data in the curve fit. Micron scale polarized FE domains were written by PFM using a Bruker Dimension 3100 Atomic Force Microscope with conductive, platinum coated tips by applying a dc voltage (writing mode) and the phase signals were observed by applying an ac voltage (reading mode).

III. RESULTS

Figure 1(a) is the atomic force microscopy (AFM) topography image of the STO substrate showing clear terraces, with a single unit-cell step height. The uniform surface termination of the substrate terraces implies a homogeneous interface between the BTO layer and the substrate over the whole sample. Two samples were prepared using different growth rates. Figures 1(b) and 1(c) show the AFM images of the BTO films after annealing at a temperature of 700 °C in O_2. The thicknesses, as estimated from the Sr-3d core-level intensities (see discussion of Sr-3d XPS, below) were 3.2 nm (sample 1) and 3.8 nm (sample 2), grown at rates of 1 and 0.5 ML/min, respectively. The film quality is different. Sample 1 has large micrometer-sized pinholes, whereas sample 2 pinholes are smaller by between one and two orders of magnitude.

Figure 2 shows the XRD scans of two BTO films. In the out-of-plane scans, the two main peaks located at $2\theta = 22.75°$
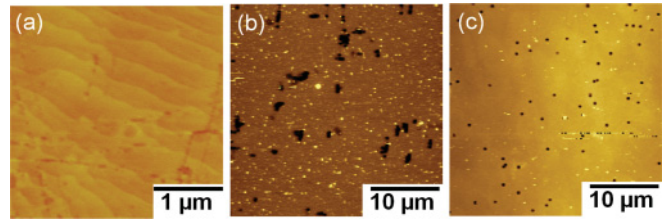

FIG. 1. (Color online) AFM topography image of (a) STO substrate (b) sample 1 (crystalline BTO film) and (c) sample 2 (QA BTO film).

and 46.48° correspond, respectively, to the STO(001) and STO(002) reflections from the substrate. For sample 1 (upper curve), structures are observed at the low 2θ angles with respect to the STO peaks position. Their calculated lattice parameter is 0.4037 nm, corresponding to that of fully relaxed BTO (0.4036 nm). The diffraction pattern of the lower growth rate film has no clear small-angle structure, although there appears to be a very slight asymmetry or shoulder toward lower 2θ angles, discussed below. Thus there is no evidence for long-range order perpendicular to the surface distinct from that of the substrate. The inset of Fig. 2 shows the in-plane XRD scans. One main peak is observed at $2\theta = 32.38°$ corresponding to the STO substrate. In the case of sample 1 (upper curve in inset), we again observe a structure on the low-angle side of the STO peak, corresponding to an in-plane lattice parameter of 0.4010 nm, consistent with fully relaxed in-plane BTO. On the other hand, the in-plane scan of sample 2 (lower curve in inset), shows no XRD peak apart from that of the STO substrate, confirming the absence of a distinct crystalline phase in this BTO film. For a thin film with a free surface, there is no possible mechanism of isotropic pressure. Thus the only explanation for the absence of a distinct XRD signal in and out of plane is that the BTO sample 2 has no long-range order, i.e., the BTO is amorphous.
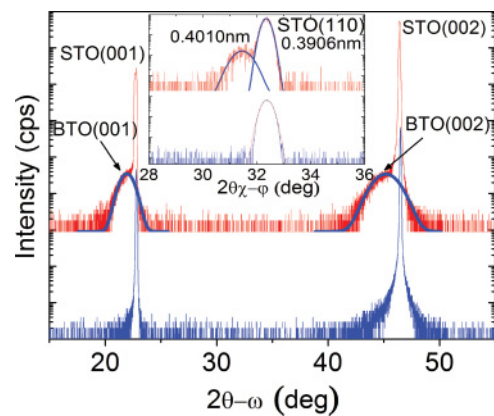

FIG. 2. (Color online) Out-of-plane scan XRD spectra of sample 1 (upper) and sample 2 (lower) subsequently identified as crystalline and quasiamorphous BTO films, respectively. The two peaks located at $2\theta = 22.75°$ and 46.48° are due to STO (001) and STO (002) reflections, respectively. (inset) In-plane scans of crystalline (upper) and quasiamorphous (lower). The STO substrate is at $2\theta = 32.38°$. The low-angle structure in the crystalline film corresponds to fully relaxed BTO, there is a slight low-angle asymmetry in the scan of the quasiamorphous film.
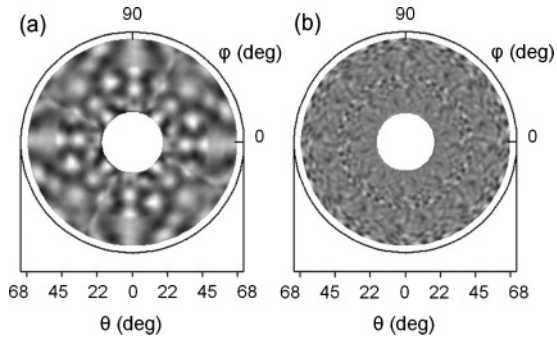
FIG. 3. Ti-2p XPD diffraction patterns from (a) crystalline BTO and (b) sample 2 (QA BTO).

In Fig. 3(a), we present the symmetrized Ti-2$p_{3/2}$ XPD patterns of a crystalline BTO film. The XPD pattern of sample 2 is presented in Fig. 3(b). In contrast to the regular diffraction pattern of the crystalline sample, which reflects the high local order, the XPD pattern of sample 2 shows no angular anisotropy. The center of XPD pattern represents normal emission; the edge represents grazing angle emission. Thus there is no macroscopically coherent local order in either in-plane or out-of-plane directions, which further reinforces the conclusion from XRD that sample 2 is amorphous. Figure 4(a) shows the phase response of the PFM-written FE domains on the amorphous film. The contrast between bright and dark areas can be clearly observed. The outer square of $40 \times 40 \ \mu m^2$ was written by a positive bias of $+6$ V creating a negative image charge below the surface and thus a downward pointing polarization (P^-) and the inner area of $20 \times 20 \ \mu m^2$ square was reversed by a -6 V bias, creating an upward pointing polarization (P^+). The contrast originating from P^+ and P^-
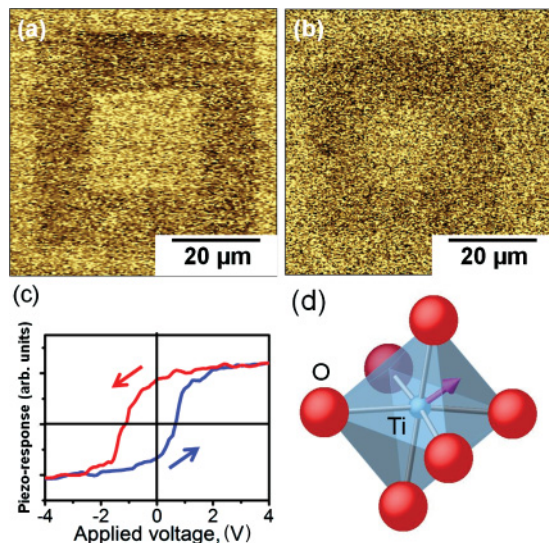

FIG. 4. (Color online) PFM phase image of sample 2 (QA BTO film) showing contrast originating from P^+ and P^- polarizations (a) immediately after writing and (b) 24 hours later. (c) Ferroelectric P-E hysteresis loop for the QA BTO film obtained 24 hours after writing. The direction around the loop is indicated by the arrows. (d) Schematic of the distorted TiO_6 octahedra in quasiamorphous BTO. The off-center Ti displacement is along $\langle 111 \rangle$, indicated by the arrow giving rise to shorter and longer Ti-O bonds.

polarizations was also observed 24 hours later [see Fig. 4(b)], excluding the possibility of significant charge injection during domain writing, minimizing artefacts due to the electrostatic interaction between the lever and the sample and confirming the remanent FE polarization. Figure 4(c) is the hysteresis of the piezoresponse obtained by ramping the applied voltage on the PFM tip obtained in the inner P^+ square of Fig. 4(b), providing clear evidence of the ferroelectric nature of the film.[11,15] If the piezo response were due to trapped charge, the hysteresis loop would be reversed. The exterior, unwritten sample area, also exhibits a net positive polarity, probably due to a FE imprint in the film. Ferroelectricity has already been observed in ultrathin crystalline BTO films though never in such a thin amorphous structure.[16,17] Figure 4(d) shows a schematic of the off-center $\langle 111 \rangle$ Ti displacement most widely reported in the literature.[18,19]

Since the volume detection limit of a crystalline phase by XRD is about 0.3%,[3,20] an order of magnitude smaller than the fraction of TiO_6 octahedra thought to contribute to the polarization in thicker QA samples[7] and since the XPD shows no macroscopically coherent local order, we can exclude the formation of nanocrystalline BTO in sample 2. The easy acquisition of a hysteresis loop by the PFM tip over all the sample surface with a high coercive field [estimated from $(||E_C| + |-E_C|)/2$ to be 2000 kV/cm, see below] also makes it highly unlikely that the ferroelectricity originates from small crystalline grains. Thus the evidence points to the formation of a polar QA phase of BTO after annealing at 700 °C in O_2 flow. From the slight asymmetry or shoulder in the out of plane XRD curve, the calculated lattice constant for the low-angle structure is 4.100 Å, much larger than that of bulk BTO. We interpret it as the result of the alignment along c axis of first BTO unit cell with the STO substrate. The Sr-3d intensities discussed below provide further support for this interpretation. The large voids or pinholes observed in AFM image of sample 1 probably result from relaxation of the BTO during postdeposition annealing, producing a fully relaxed, crystalline film. The transition from amorphous to crystalline state requires a considerable volume expansion prior to nucleation.[6] If the expansion is frustrated, then a QA phase results. Hence, sample 2 may form a QA phase due to the in-plane clamping by the STO substrate which would also explain the very small pinholes. Hereafter, we will refer to samples 1 and 2 as the crystalline and the quasiamorphous (QA) films, respectively.

The C-1s, Ti-2p, Ba-3d, O-1s, and Sr-3d core-level XPS spectra are shown in Figs. 5(a)–5(e). The intensity of the C-1s spectra in Fig. 5(a) shows that both thin film surfaces have a similar low carbon contamination. More importantly, the high-binding-energy component usually associated with carbonate-like bonding at the surface is 12 times weaker than the main C-1s peak. This indicates that the surface is indeed largely free of carbonate adsorbates that could affect the ferroelectricity. In careful studies of clean BTO surfaces, for example, Baniecki *et al.*,[21] the carbonate peak is typically ten times smaller than the main C-1s line.

The Ti-2$p_{3/2}$ spectra are shown in Fig. 5(b). The spectra are fitted with the same FWHM (1.0 eV) and Gaussian/Lorentzian (70/30) ratio for all peaks. Thanks to the high energy resolution, we see that the two spectra are not identical, unlike
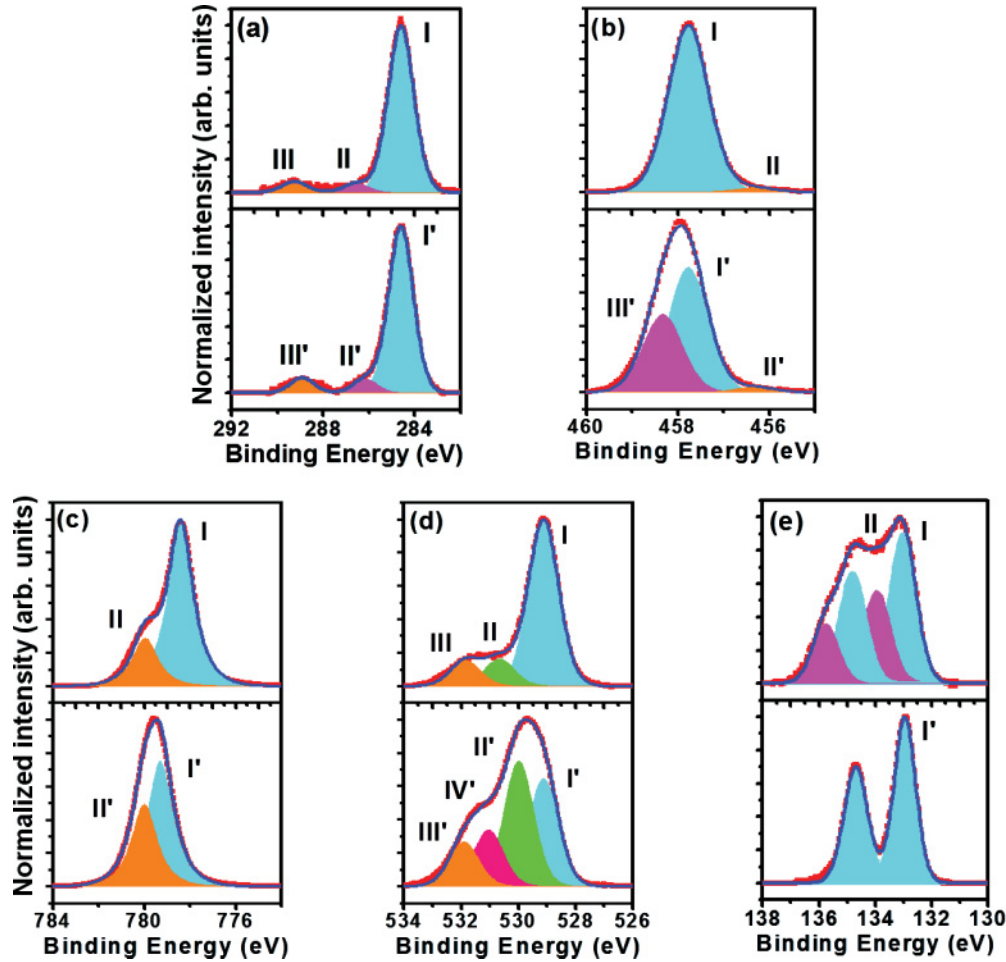
FIG. 5. (Color online) Core-level spectra for crystalline (top) and QA (bottom) films: (a) C-1s, (b) Ti-2$p_{3/2}$, (c) Ba-3$d_{5/2}$, (d) O-1s, and (e) Sr-3d spectra from the STO substrate under the films.

previous work[10] on much thicker films (50–200nm). Both crystalline and QA spectra have a main component due to Ti with a formal valency of 4+ in the TiO_6 octahedra, and a very weak, low-binding-energy (LBE) component corresponding to reduced Ti, often described as Ti^{3+}. The latter is known to occur as a result of the formation of oxygen vacancies, the presence of which is confirmed by the valence band spectra shown below (see Fig. 6). There is no observable shift in the main peak between crystalline and QA samples in agreement with Ref. 10, demonstrating that the TiO_6 LBUs are largely chemically unchanged, consistent with EXAFS analysis of QA STO and BTO.[7,9] However, the intensity decreases significantly in the QA spectrum with the simultaneous appearance of a high-binding-energy (HBE) component shifted by 0.5 eV with respect to the main peak. The HBE component we observe in the QA spectrum is reminiscent of the HBE component observed in Ba-3d spectra of crystalline BTO films.[21,22] This has been associated with a near surface space charge region giving rise to charge depletion[23] and is discussed below.

The XPS spectra of Ba-3$d_{5/2}$ and O-1s are presented in Figs. 5(c) and 5(d). Both the shape and the position of the Ba-3$d_{5/2}$ line change when going from crystalline to QA. In the former, the main peak, labeled I, has a binding energy of 778.4 eV, in the QA sample the peak shifts by 0.9 eV

to higher BE. Each spectrum also has an HBE component labeled II, shifted by 1.6 and 0.7 eV for crystalline and QA BTO, respectively. Grazing emission angle XPS (not shown) confirmed that this HBE component is of surface origin. The shift of the surface component in crystalline BTO is very similar to that observed on the clean surface of a thick BTO single-crystal film and characteristic of the FE state.[21] It should be recalled that there is no evidence for the presence of significant surface carbonate species therefore the HBE component cannot be attributed to $BaCO_3$ species. The O-1s spectra also show important differences when going from crystalline to QA films. The spectrum of the crystalline film can be deconvoluted into three components, peak I due to oxygen in the perovskite environment, and peaks II and III, both of which are of surface origin. Peak II is shifted by 1.6 eV with respect to peak I, similar to the clean surface related shift in the Ba 3d, whereas peak III is at a binding energy of 531.9 eV and is ascribed to low residual surface contamination. On the other hand, the QA spectrum requires four peaks to achieve a good fit. Components I and III are unshifted with respect to the crystalline film, unlike the main Ba-3d component in Fig. 5(c). Peak II, of surface origin, is shifted by 0.9 eV with respect to the main component instead of 1.6 eV in the case of the c film. The origin of the fourth peak is still under

investigation. However, its presence suggests that there is not a simple symmetry based on static charge transfer between oxygen and cations in the QA amorphous phase, but rather a more complex change in atomic and electronic structure. The Sr-3d spectra from the substrate of crystalline and QA films are presented in Fig. 5(e). The positions of the main Sr-3d peak of both samples, labeled I, are indistinguishable within the experimental accuracy. The spectrum of the crystalline film has an HBE component, labeled II, shifted by 0.9 eV. The appearance of surface component is also observed on clean STO surfaces.[21,24] In our case, there is no free STO surface, however, the finite XPS probing depth means that the Sr-3d spectra are particularly sensitive to the chemical environment at the BTO/STO interface. Thus the Sr at the interface with the QA film appears to be in a bulklike environment, whereas the Sr at the interface with the fully relaxed crystalline BTO has a similar spectrum to that of a clean STO surface. This would indeed be consistent with the interpretation of the out-of-plane XRD scan of the QA sample being due to the epitaxy of the first BTO unit cell on the STO surface. The full relaxation of the crystalline BTO film, on the other hand, reduces sufficiently the chemical bonding at the interface so that the Sr-3d spectrum shows a more surfacelike character. The Sr-3d intensity has been used to estimate the thickness of the crystalline and QA BTO films to be 3.2 and 3.8 nm, respectively. The mean-free path has been calculated using the National Institute of Standards and Technology (NIST) database,[25] and as a first approximation we have assumed BTO films with the bulk mass density. A more accurate calculation would have to take into account volume change, but the observed pinhole concentration makes this adjustment difficult.

The valence band spectra are reported in Fig. 6. They are very similar to crystalline and QA results obtained on much thicker films.[10] All of the features reported in Ref. 10 are visible in the spectra. The double-peak structure at 3.3 and 5.1 eV corresponds to O-2π and σ bonding orbits. The peaks are less well resolved in the QA phase because of structural disorder.[26,27] There is also a broad peak between 8.6 and 11.2 eV in the QA spectrum, which is absent from the crystalline phase. Density functional theory (DFT) calculations have shown that there is a significant contribution to the density of states (mainly, O p_z projected) in this region due to the additional O-O coordination in BaO_2 compared to
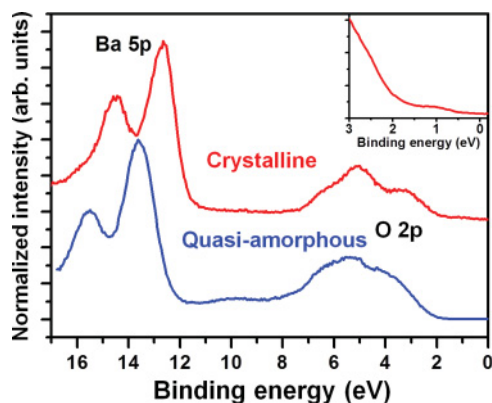

FIG. 6. (Color online) Valence band spectra of the crystalline and QA BTO. (Inset) Fermi-level region of the crystalline BTO film.

BaO.[28] The combination of apex, edge, and even face sharing TiO_6 octahedra in amorphous and QA phases would produce such Ba-mediated O-O coordination, as discussed in Ref. 6, although as yet only evidence for apex and edge sharing has been furnished.[9] Note also that the Ba-5p semicore levels are shifted by about 1 eV to higher binding energy just like the Ba 3d shown in Fig. 5(c). The density of states observed in the band-gap region just over 1 eV below the Fermi level corresponds to oxygen vacancy states, consistent with the small component due to reduced Ti observed in Fig. 5(b).

IV. DISCUSSION

In QA phase, the distorted TiO_6 LBUs can, in principle, be connected in three different ways: apex to apex, edge to edge, and face to face, although as previously mentioned, the latter case has yet to be demonstrated. Ba ions are located in the voids created between the distorted LBUs. The Ba ions in such bonds must have less than 12 O neighbors and should therefore have some excess negative charge compared with the perovskite BTO. Simultaneously, some of the TiO_6 corners must be unconnected and the oxygen at these apices has only one Ti neighbor, acquiring some excess positive charge. The significant decrease of peak I intensity at 529.1 eV and appearance of a new peak IV at HBE for O-1s line are an indication of a major structural change in the perovskite structure.

A simple interpretation based on static charge transfer cannot explain all the observed behavior. For example, the Ba-3d peaks are shifted when going from the crystalline to QA film, whereas the O-1s show in addition, a new HBE component. Static charge transfer can give a first insight into, for example, the valence state of ions or the chemical bonding. However, one would expect reciprocity in at least the direction of the core-level shifts between an anion and a cation involved in charge transfer. Exact charge transfer is difficult to measure because it is always, to some extent, arbitrary, in particular, in correlated systems like ferroelectrics. Dynamical charge is more relevant for deformed polar materials.[29] First principles calculations of the Born effective charge (i.e., in the absence of an external electric field) allow band-by-band analysis of the contributions to the anomalous dynamical charge as a function of the atomic distortion. Using this method, Ghosez *et al.*[29] have shown that the electronic current flows opposite to the displacement of positive ions enhancing the change in polarization. Contrary to a simple charge transfer model, the dynamical charge tensor is not just a function of the shortest or longest Ti-O bond, but rather of the anisotropy along the Ti-O chains. In this picture, the shorter Ti-O bonds will have enhanced covalency, whereas the longer bonds will be more ionic. Thus the partially covalent character of Ti-O bonds in perovskite oxides[24,30] will certainly be modified by the high off-center Ti position creating a strong anisotropy in the Ti-O bond length along the *c* axis of each octahedron. This may explain why we also observe a surface-related peak at HBE in the QA Ti-2p spectrum just like in the Ba-3d spectrum. In the presence of higher ionicity, a stronger space-charge effect at the surface may be expected, giving rise to a similar shift in the Ti-$2p_{3/2}$ peak. To our knowledge, such a component has not been previously observed in crystalline BTO and seems to be specific to the ultrathin QA layer. Both O-1s

and Ba-3*d* surface-related peaks are less shifted with respect to the main peak in the QA film than in the crystalline film. We think that the lack of long-range order results in a less well defined microscopic boundary condition of the displacement field at the surface than for a crystalline film. The breaking of the long-range order by the quasiamorphous structure renders an understanding of the local polarization induced by atomic distortion even more important. The link between microscopic structure and macroscopic polarization in ferroelectrics has long been a matter of debate with both displacive[31] and order-disorder eight-site[18] models proposed. Recent quantum-mechanical calculations using density functional theory,[19] based on original insights into the interaction between long wavelength soft phonon modes and local atomic distortion,[32] integrate antiferroelectricity into the ferroelectric phases of BTO to satisfactorily explain XAS,[33] Raman,[34] and IR[35] experiments. Thus the off-center Ti displacement is now thought to be along ⟨111⟩ with local order between adjacent chains of TiO$_6$ octahedra. However, in our case, there is no long-range order, therefore the observed polarization can only be due to a preferential alignment of the local distortion in the TiO$_6$ octahedra.

Nevertheless, some useful insights may be obtained by comparing the coercive field measured here with that measured or calculated for crystalline thin films. In strained crystalline thin films, using the free energy density functional of homogeneous switching in the out-of-plane polarization state ($P_1 = P_2 = 0$, $P \neq 0$) within a nonlinear thermodynamic theory, the coercive field is calculated to be 1600 kV/cm.[36] The coercive field, E_C, obtained from ferroelectric hysteresis loop measured on the QA BTO film is 2000 kV/cm in a parallel plate capacitor geometry. This is about eight times larger than that observed of BTO on SrRuO$_3$ (SRO),[37] which has a similar compressive strain (2.2%). Jo *et al.* showed that when the domain nucleation shape changes from half prolate spheroidal to cylindrical in thin films, the calculated coercive field is reduced from 700 to 250 kV/cm for a thickness of 4 nm,[37] in agreement with their experiment. The lack of long-range order in the quasiamorphous film makes the presence of such cylindrical domains energetically unfavorable, thus a higher coercive field is probable, possibly pointing to spheroidal domain nucleation as the switching mechanism. This is further circumstantial evidence that the macroscopic polarization observed in the quasiamorphous structure does not include a long-range displacive contribution and is, in fact, due to the sum of local, distortion-induced polarizations.

As previously noted, BTO must undergo a volume expansion of about 10% prior to the onset of nucleation and crystallization.[6] Due to in-plane clamping, volume expansion is frustrated. The Ti ions shifted 0.44 Å off center in the TiO$_6$ octahedra along the *c* axis, almost twice as big as in the room-temperature crystalline FE phase (0.23 Å),[7] changing the anomalous dynamical charge and hence the local polarization. The presence of a local atomic distortion is not, in itself, a sufficient condition for macroscopic polarization that requires a preferential orientation of the LBUs imposed by the in-plane clamping. Our measured coercive field would represent 4−5% of aligned LBUs in a single-crystal film. For a macroscopic polarization equal to the sum of the local polarizations, the figure is most probably significantly higher. However, it is

clear that a detailed understanding of how local polarization can give rise to ferroelectricity in an amorphous structure is far from complete. The exact stoichiometry, for example, may also play an important role.

Compared with the method previously used,[3,4] the one presented here is more suitable for preparation of QA ultrathin BTO films. To form a crystalline phase, an amorphous film must first undergo volume expansion upon heating, turning into an intermediate low-density phase before crystallization. If the film is clamped by a substrate, then in-plane volume expansion is blocked, nucleation may be suppressed resulting in the QA phase.[38] The lattice mismatch between the STO substrate and BTO is smaller than for Si or SiO$_2$, possibly reducing the dislocation density in the film, which could otherwise provide nucleation sites. The key factor in the production of such a QA film seems to be the appropriate growth rate followed by clamping control during annealing in oxygen. We think that this is the reason why we can anneal the whole STO substrate-supported film directly rather than using a pull through a narrow hot zone. Finally, we note that the observed phenomenon may turn out to be more generally applicable in the case of ultrathin amorphous films, offering some interesting new physics.

V. CONCLUSION

We have identified the ferroelectric phase in a quasiamorphous ultrathin BTO film grown on STO(001) substrate at room temperature by MBE. In-plane clamping prevents nucleation of the as-deposited amorphous BTO during annealing in O$_2$ flow and results in the formation of a QA phase. The QA nature is confirmed by in- and out-of-plane XRD, XPD, and XPS. Significant changes in the electronic structure are observed compared with an ultrathin crystalline film. In the QA phase, Ba ions occupy voids between distorted octahedral LBUs changing the observed core-level binding energies. A new component is observed in the Ti-2$p_{3/2}$ core-level spectrum, which we qualitatively interpret on the basis of dynamical charge arguments. The valence band spectra are identical to those previously observed in much thicker films. FE polarized domains with good retention have been successfully written into the QA film and the FE nature is proven by a clear *P-E* hysteresis curve. In the literature, the QA phase was generated from the strain induced by pulling through a high temperature gradient, whereas here the strain state is governed by surface clamping. These results demonstrate the preparation of a QA FE BTO thin film grown on STO substrate by uniform post-deposition annealing.

*nick.barrett@cea.fr

[1] R. Ramesh and D. G. Schlom, Science **296**, 1975 (2002).

[2] C. H. Ahn, K. M. Rabe, and J.-M. Triscone, Science **303**, 488 (2004).

[3] V. Lyahovitskaya, I. Zon, Y. Feldman, S. R. Cohen, A. K. Tagantsev, and I. Lubomirsky, Adv. Mater. **15**, 1826 (2003).

[4] D. Ehre, V. Lyahovitskaya, A. Tagantsev, and I. Lubomirsky, Adv. Mater. **19**, 1515 (2007).

[5] D. Ehre, H. Cohen, V. Lyahovitskaya, A. Tagantsev, and I. Lubomirsky, Adv. Funct. Mater. **17**, 1204 (2007).

[6] E. Wachtel and I. Lubomirsky, Adv. Mater. **22**, 2485 (2010).

[7] A. I. Frenkel, Y. Feldman, V. Lyahovskaya, E. Wachtel, and I. Lubomirsky, Phys. Rev. B **71**, 024116 (2005).

[8] V. Lyahovitskaya, Y. Feldman, I. Zon, E. Wachtel, K. Gartsman, A. K. Tagantsev, and I. Lubomirsky, Phys. Rev. B **71**, 94205 (2005).

[9] A. I. Frenkel, D. Ehre, V. Lyahovitskaya, L. Kanner, E. Wachtel, and I. Lubomirsky, Phys. Rev. Lett. **99**, 215502 (2007).

[10] D. Ehre, H. Cohen, V. Lyahovitskaya, and I. Lubomirsky, Phys. Rev. B **77**, 184106 (2008).

[11] H. Fujisawa, M. Shimizu, H. Niu, H. Nonomura, and K. Honda, Appl. Phys. Lett. **86**, 012903 (2005).

[12] A. Pancotti, N. Barrett, L. F. Zagonel, and G. M. Vanacore, J. Appl. Phys. **106**, 034104 (2009).

[13] M. Kawasaki, K. Takahashi, T. Maeda, R. Tsuchiya, M. Shinohara, O. Ishiyama, T. Yonezawa, M. Yoshimoto, and H. Koinuma, Science **266**, 1540 (1994).

[14] [http://www.casaxps.com/].

[15] O. Kolosov, A. Gruverman, J. Hatano, K. Takahashi, and H. Tokumoto, Phys. Rev. Lett. **74**, 4309 (1995).

[16] N. Sai, A. M. Kolpak, and A. M. Rappe, Phys. Rev. B **72**, 020101 (2005).

[17] V. Garcia, S. Fusil, K. Bouzehouane, S. Enouz-Vedrenne, N. D. Mathur, A. Barthélémy, and M. Bibes, Nature (London) **460**, 81 (2009).

[18] R. Comès, M. Lambert, and A. Guinier, Acta Crystallogr. Sect. A **26**, 244 (1970).

[19] Q. Zhang, T. Cagin, and W. A. Goddard III, Proc. Natl. Acad. Sci. USA **103**, 14695 (2006).

[20] B. K. Tanner, *X-Ray Diffraction topography* (Pergamonn Press, Oxford, 1976).

[21] J. D. Baniecki, M. Ishii, T. Shioga, K. Kurihara, and S. Miyahara, Appl. Phys. Lett. **89**, 162908 (2006).

[22] N. Barrett, J. Rault, I. Krug, B. Vilquin, G. Niu, B. Gautier, D. Albertini, P. Lecoeur, and O. Renault, Surf. Interface Anal. **42**, 1690 (2010).

[23] X. L. Li, H. B. Lu, Ming Li, Zhenhong Mai, Hyunjung Kim, and Q. J. Jia, Appl. Phys. Lett. **92**, 012902 (2008).

[24] G. M. Vanacore, L. F. Zagonel, and N. Barrett, Surf. Sci. **604**, 1674 (2010).

[25] C. J. Powell and A. Jablonski, J. Phys. Chem. Ref. Data **28**, 19 (1999).

[26] Y. Adachi, S. Kohiki, K. Wagatsuma, and M. Oku, J. Appl. Phys. **84**, 2123 (1998).

[27] L. T. Hudson, R. L. Kurtz, S. W. Robey, D. Temple, and R. L. Stockbauer, Phys. Rev. B **47**, 1174 (1993).

[28] M. Königstein, A. A. Sokol, and C. R. A. Catlow, Phys. Rev. B **60**, 4594 (1999).

[29] Ph. Ghosez, J.-P. Michenaud, and X. Gonze, Phys. Rev. B **58**, 6224 (1998).

[30] H. Wadati, A. Maniwa, A. Chikamatsu, H. Kumigashira, M. Oshima, T. Mizokawa, A. Fujimori, and G. A. Sawatzky, Phys. Rev. B **80**, 125107 (2009).

[31] W. Cochran, Adv. Phys. **9**, 387 (1960).

[32] Y. Girschberg and Y. Yacoby, Solid State Commun. **103**, 425 (1997).

[33] B. Ravel, E. A. Stern, R. I. Vedrinskii, and V. Kraizman, Ferroelectrics **206**, 407 (1998).

[34] H. Vogt, J. A. Sanjurjo, and G. Rossbroich, Phys. Rev. B **26**, 5904 (1982).

[35] Y. Luspin, J. L. Servoin, and F. Gervais, J. Phys. C **13**, 3761 (1980).

[36] N. A. Pertsev, A. G. Zembilgotov, and A. K. Tagantsev, Phys. Rev. Lett. **80**, 1988 (1998).

[37] J. Y. Jo, Y. S. Kim, T. W. Noh, Jong-Gul Yoon, and T. K. Song, Appl. Phys. Lett. **89**, 232909 (2006).

[38] I. Ebralidze, V. Lyahovitskaya, I. Zon, E. Wachtel, and I. Lubomirsky, J. Mater. Chem. **15**, 4258 (2005).